



Higher-Order Sliding Mode Control of a Wind Energy Conversion System

S. Boulkhrachef¹, A. Moualdia^{1*}, DJ. Boudana¹ and P. Wira²

¹ Laboratory of Electrical Engineering and Automatics (LREA), University of Medea, Algeria

² Laboratory of Modeling Intelligence Process Systems, University of Haute-Alsace (MIPS), Mulhouse, France

Received: July 9, 2019; Revised: September 30, 2019

Abstract: This work presents a control strategy employing the second-order sliding mode for a variable-speed wind energy system based on a double-fed asynchronous machine (DFIG). This technique finds its stronger justification in the problem of using a nonlinear control law robust to inaccuracies in the model. The objective is to apply this command to independently control the active and reactive power generated by the double-fed asynchronous machine decoupled from the flow direction. The use of this method provides very satisfactory performance for the DFIG control. The overall strategy has been validated on a 7.5 kW wind turbine driven by a DFIG using the Matlab/Simulink. The numerical simulation results show the growing importance of this control in the systems of wind energy conversion.

Keywords: DFIG; PWM converters; MPPT, higher-order sliding mode controller; wind energy.

Mathematics Subject Classification (2010): 03B52, 93C42, 94D05.

1 Introduction

The consumption of electricity has increased dramatically over the past decade because of the massive industrialization of some countries and the significant population increase. During the first half of the century, fossil fuels remain the main source of energy, which consequently causes environmental problems in terms of global warming and climate change. Nowadays, the renewable energy attracted the interest of several research teams. Thus, the development of wind turbines is a great investment in technological research.

* Corresponding author: <mailto:amoualdia@gmail.com>

Among these sources of renewable energy, wind energy has the greatest energy potential. With the power of wind turbines installed around the world increasing every year, wind systems can no longer act as active power generators in distribution or transmission networks, depending on the installed capacity. Indeed, they will certainly be led, in the short term, to provide system services (reactive power compensation, for example) such as conventional power plant generators and / or to participate in the improvement of the quality of electrical energy (filtering harmonic currents, in particular). Much of the wind turbines installed today are equipped with a double-fed induction machine (DFIG) [1, 2].

This generator allows power generation variable speed; this then allows better use of wind resources under different wind conditions. These turbines are also equipped with a propeller-pitch blade to accommodate variable wind conditions. The entire wind turbine is controlled to maximize the power produced continuously searching for the operating point at maximum power commonly called MPPT. However, this type of energy is an energy booster in relation to nuclear generation and remains largely predominant in many works presenting the DFIG with diverse control diagrams. These control diagrams are frequently based on the vector control notion with sliding mode controllers as proposed in [2, 3].

In the electromechanical conversion chain of a wind turbine system, three-phase static voltage converters are essential elements because they make it possible to control the active and reactive powers injected into the electrical network as a function of the wind speed applied to the wind turbine blades.

In recent years, the sliding mode control (SMC) methodology has been widely used for the control of nonlinear systems. It achieves a robust control by adding a discontinuous control signal across the sliding surface, satisfying the sliding condition. Nevertheless, this type of control has an essential disadvantage, which is the chattering phenomenon caused by the discontinuous control action. To treat these difficulties, several modifications to the original sliding mode control law have been proposed, the most common and recent strategy is using a second order sliding mode controller as in [1, 2].

The proposed control strategy is a second-order sliding mode for the DFIG control. This strategy possesses attractive features such as the chattering-free behavior and robustness. This work is organized as follows. In Section 2, we briefly review the modeling of the whole system under study. Section 3 provides the detail of the second-order sliding mode control technique and its application to the DFIG control.

The system under study is shown in Figure 1. This farm consists of three aero-generators, where each one is connected to a variable-speed asynchronous generator. For operation at variable speed, three rectifiers are used to connect the generators to the DC bus. This bus is linked to the electrical network via a tow level inverter and an RL (resistance R and inductor L) filter. The subject of this paper consists in designing control strategies for a wind energy conversion system, connected to the network based on the rotor-powered dual-power asynchronous machine via two reversible PWM converters (one rotor side and the other network side) in back-to-back mode, realizing the electrical interface between the rotor of the machine and the network. The control of the latter consists in regulating the intermediate DC bus regardless of the power generated by the conversion system under variable frequency.

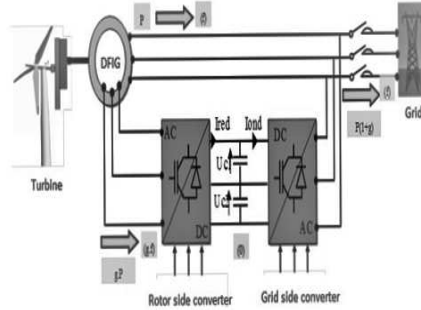


Figure 1: The overall pattern of a chain of wind energy conversion.

2 System Model

2.1 Wind turbine model

For a horizontal axis wind turbine, the mechanical power captured from the wind is given by [14]

$$P_t = \frac{1}{2} C_p(\lambda, \beta) R^2 \rho V^3, \quad (1)$$

where R is the radius of the turbine in (m), ρ is the air density (kg/m^3), V is the wind speed (meter/second), and (C_p) is the power coefficient which is a function of both the tip speed ratio λ and the blade pitch angle β (degree). In this work, the (C_p) equation is approximated using a non-linear function according to [15]

$$C_p = (0.5 - 0.167)(\beta - 2) \sin \left[\frac{\pi(\lambda + 0.1)}{18.5 - 0.3(\beta - 2)} \right] - 0.0018(\lambda - 3)(\beta - 2). \quad (2)$$

The tip speed ratio λ is given by

$$\lambda = \frac{R\Omega_t}{V}, \quad (3)$$

where Ω_t is the angular velocity of the wind turbine.

2.2 The DFIG model

The application of the Park transformation to the three-phase model of the DFIG permits to write the dynamic voltages and fluxes equations in an arbitrary dq reference frame:

$$\begin{cases} V_{sd} = R_s i_{sd} + \frac{d}{dt} \Phi_{sd} - \omega_s \Phi_{sq}, \\ V_{sq} = R_s i_{sq} + \frac{d}{dt} \Phi_{sq} + \omega_s \Phi_{sd}, \\ V_{rd} = R_r i_{rd} + \frac{d}{dt} \Phi_{rd} - \omega_r \Phi_{rq}, \\ V_{rq} = R_r i_{rq} + \frac{d}{dt} \Phi_{rq} + \omega_r \Phi_{rd}, \end{cases} \quad (4)$$

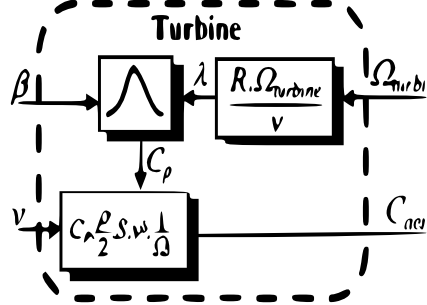


Figure 2: Turbine model.

$$\begin{cases} \Phi_{sd} = L_s i_{sd} + M i_{rd}, \\ \Phi_{sq} = L_s i_{sq} + M i_{rq}, \\ \Phi_{rd} = L_r i_{rd} + M i_{sd}, \\ \Phi_{rq} = L_r i_{rq} + M i_{sq}. \end{cases} \quad (5)$$

The stator and rotor angular velocities are linked by the following relation: $\omega_s = \omega + \omega_r$, where ω_s is the electrical pulsation of the stator and ω_r is the rotor one, ω is the mechanical pulsation of the DFIG. This electrical model is completed by the mechanical equation

$$C_{em} = C_r + J \frac{d\Omega}{dt} + f\Omega, \quad (6)$$

where C_r is the resisting torque, Ω is the mechanical speed of the DFIG, J is the inertia, f is the viscous friction and p is the number of the pairs of poles. In the two-phase reference, the stator active and reactive power of induction generator is written as

$$\begin{cases} P_s = V_{sd} i_{sd} + V_{sq} i_{sq}, \\ Q_s = V_{sq} i_{sd} - V_{sd} i_{sq}. \end{cases} \quad (7)$$

The wind farm is controlled to extract the maximum power available. According to the Betz theory, the power coefficients C_p do not exceed 0.593 [12,13], which corresponds to the Betz limit. Therefore, the power produced by a turbine is 59.3 % of the available power of wind. In this case, the variation of C_p as a function of λ for $\beta = 0$ is shown in Figure 4, then the maximum value of C_p ($C_{pmax} = 0.45$) corresponds to the optimal value of λ ($\lambda_{opt} = 8.1$). The electromagnetic torque reference given by the MPPT strategy is defined by equation (7).

$$C_{em-Opt} = \frac{C_p \rho \pi R^5 \Omega_{mec}^2}{2 \lambda_{opt}^3 G^3}. \quad (8)$$

3 Control Strategy of the DFIG

3.1 Active and reactive power decoupling

In order to easily control the production of electricity by the wind turbine, we will carry out an independent control of active and reactive powers by orientation of Φ_s . By choosing a reference frame linked to Φ_s , rotor currents will be related directly to the

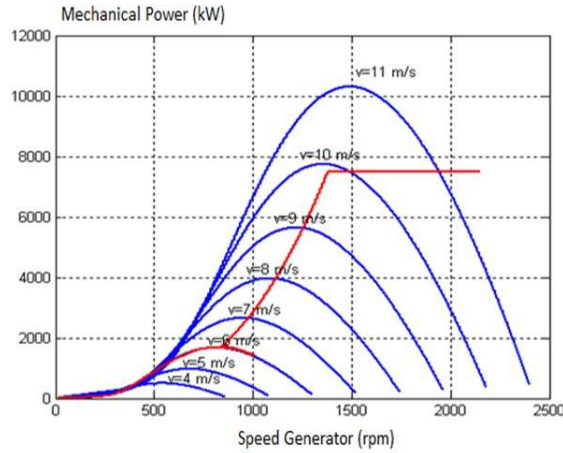


Figure 3: Mechanical power variation.

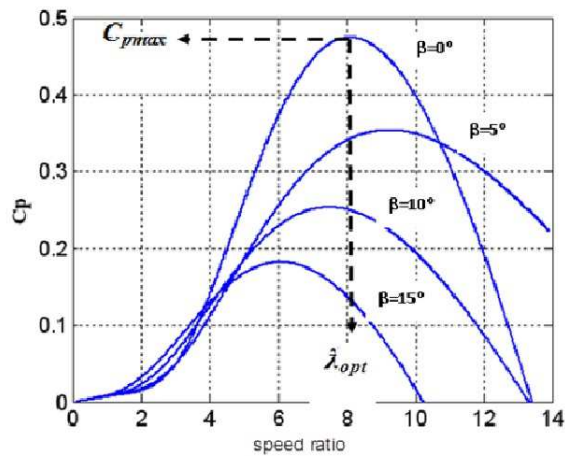


Figure 4: Power coefficient versus λ curve.

stator active and reactive power. An adapted control of these currents will thus permit to control the power exchanged between the stator and the grid. If the Φ_s is linked to the d-axis of the frame, we have

$$\begin{cases} \Phi_{sd} = \Phi_s, \\ \Phi_{sq} = 0. \end{cases} \quad (9)$$

The electromagnetic torque can then be expressed as follows:

$$C_{em} = p \frac{M}{L_s} \Phi_s i_{sq}. \quad (10)$$

By substituting (8) in (5), the following rotor flux equations are obtained:

$$\begin{cases} \Phi_s = L_s i_{sd} + M i_{rd}, \\ 0 = L_s i_{sq} + M i_{rq}. \end{cases} \quad (11)$$

In addition, the stator voltage equations are reduced to

$$\begin{cases} V_{sd} = R_s i_{sd} + \frac{d}{dt} \Phi_s d, \\ V_{sq} = R_s i_{sq} + \omega_s \Phi_s. \end{cases} \quad (12)$$

If the per-phase stator resistance is neglected, which is a realistic approximation for medium power machines used in the wind energy conversion, and by supposing that the electrical supply network is stable, for a simple voltage constant V_s we will have a constant stator flux ϕ_s constant. This consideration associated with (11) shows that the new stator voltage expressions can be written as follows:

$$\begin{cases} V_{sd} = 0, \\ V_{sq} = \omega_s \Phi_s. \end{cases} \quad (13)$$

Using (10), a relation between the stator and rotor currents can be established:

$$\begin{cases} i_{sd} = -\frac{M}{L_s} i_{rd} + \frac{\phi_s}{L_s}, \\ i_{sq} = -\frac{M}{L_s} i_{rq}. \end{cases} \quad (14)$$

By using (4), (5), (13) and (14), the stator active and reactive powers, the rotor fluxes and the rotor voltages can be written versus rotor currents as

$$\begin{cases} P_s = -\frac{M \omega_s \Phi_s}{L_s} i_{rq}, \\ Q_s = -\frac{M \omega_s \Phi_s}{L_s} i_{rd} + \frac{\omega_s \phi_s^2}{L_s}, \end{cases} \quad (15)$$

$$\begin{cases} \phi_{rd} = \sigma L_r i_{rd} + \frac{L_m \phi_s}{L_s}, \\ \phi_{rq} = \sigma L_r i_{rq}, \end{cases} \quad (16)$$

$$\begin{cases} V_{rd} = R_r i_{rd} + \sigma L_r \frac{d}{dt} i_{rd} - \sigma \omega_s L_r i_{rq}, \\ V_{rq} = R_r i_{rq} + \sigma L_r \frac{d}{dt} i_{rq} + \sigma g \omega_s L_r i_{rd} + \omega_s \frac{L_m \phi_s}{L_s}. \end{cases} \quad (17)$$

3.2 Second-order sliding mode power control of the DFIG

The sliding mode control (SMC) is one of the most interesting nonlinear control approaches. Nevertheless, a few drawbacks arise in its practical implementation, such as the chattering phenomenon and undesirable mechanical effort. In order to reduce the effects of these problems, a high-order sliding mode seems to be a very attractive solution. This method generalizes the essential sliding mode idea by acting on the higher-order time derivatives of the sliding manifold instead of influencing the first time derivative as

in the case of the SMC [10, 18]. The main feature of this control is that it only needs to drive the error to a switching surface. In this study, the errors between the measured and reference d and q rotor currents have been chosen as sliding mode surfaces, so the following expression can be written:

$$\begin{cases} S_d = i_{rd-ref} - i_{rd}, \\ S_q = i_{rq-ref} - i_{rq}. \end{cases} \quad (18)$$

Replacing the d and q rotor currents derivatives in (18) by their expressions taken from (17), one obtains

$$\begin{cases} \dot{S}_d = \dot{i}_{rd-ref} - \dot{i}_{rd} = \frac{1}{L_r\sigma} V_{rd} + \frac{1}{L_r\sigma} (-R_r i_{rd} + g\omega_s L_r \sigma i_{rq}) + \dot{i}_{rd-ref}, \\ \dot{S}_q = \dot{i}_{rq-ref} - \dot{i}_{rq} = \frac{1}{L_r\sigma} V_{rq} + \frac{1}{L_r\sigma} \left(-R_r i_{rd} + g\omega_s L_r \sigma i_{rd} - g\omega_s \phi_s \frac{L_m}{L_s} \right) + \dot{i}_{rq-ref}. \end{cases} \quad (19)$$

For the sliding mode surfaces given by (20), the following expression can be written:

$$\begin{cases} \ddot{S}_d = \wedge_1(t, x) V_{rd} + Y_1(t, x), \\ \ddot{S}_q = \wedge_2(t, x) V_{rq} + Y_2(t, x), \end{cases} \quad (20)$$

where $\wedge_1(t, x)$, $\wedge_2(t, x)$, $Y_1(t, x)$ and $Y_2(t, x)$ are uncertain functions which satisfy

$$\begin{cases} Y_1 > 0, |Y_1| > \lambda_1, 0 < K_{m1} < \wedge_1 < K_{M1}, \\ Y_2 > 0, |Y_2| > \lambda_2, 0 < K_{m1} < \wedge_2 < K_{M2}. \end{cases} \quad (21)$$

We define the same higher-order slip surfaces considered for power control design:

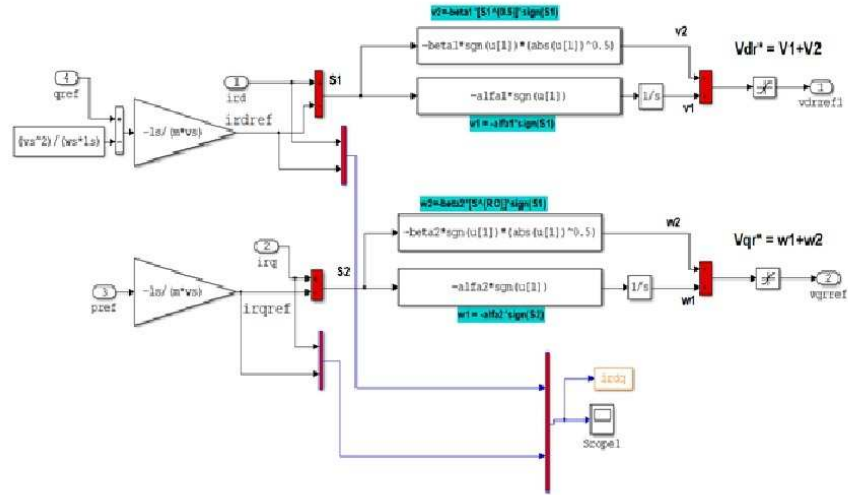
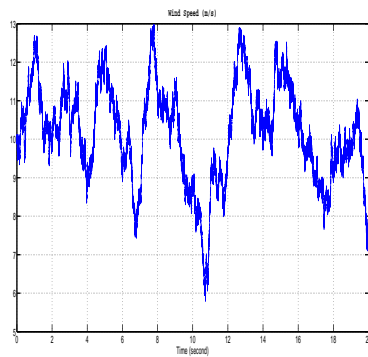
$$\begin{cases} \dot{S}_1 = F.V_{rd} + G_1, \\ \dot{S}_2 = F.V_{rq} + G_2. \end{cases} \quad (22)$$

Based on the algorithm of super twisting introduced by Levant in [12], one proposes the following command [15]:

$$\begin{cases} V_{rd} = \alpha_1 \int sign(S_1) dt + \beta_1 |S_1|^{0.5} sign(S_1), \\ V_{rq} = \alpha_2 \int sign(S_2) dt + \beta_2 |S_2|^{0.5} sign(S_2). \end{cases} \quad (23)$$

4 Simulation Results

In the objective to evaluate the performances of the *second – order* sliding mode controller, simulation tests are realized with a 7.5 kW generator coupled to a 400V/50 Hz grid. Simulation of the whole system has been realized using Matlab/Simulink. Figure 6 illustrates the waveforms of the wind profile used in the simulation. In this figure, the wind speed is around 13 (*m/s*) which corresponds to the maximum power generation. Figure 7 shows also that the stator current obtained by the DFIG has a sinusoidal form, which implies a clean energy without harmonics provided by the DFIG. Figure 8 shows the simulation results of the whole system given by the bloc diagram in Figure 1. This diagram presents a DFIG model associated with a wind turbine which is controlled by

**Figure 5:** Algorithm of super twisting.**Figure 6:** Wind speed profile.

the MPPT (Maximum Power Point Tracking) strategy. As is shown in this figure, for a variable wind speed, the stator active power produced by the DFIG is controlled according to the MPPT strategy and is around 7.5 kW, which represents the nominal power of the DFIG while the stator reactive power is maintained to zero. In addition, it can be noticed that the direct and quadrature rotor current take the same forms as the stator reactive and active power, respectively, as shown in Figure 9.

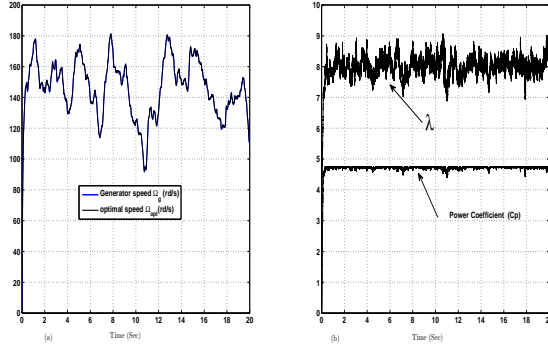


Figure 7: MPPT results: (a) generator speed, (b) coefficient power C_p and the speed ratio (λ).

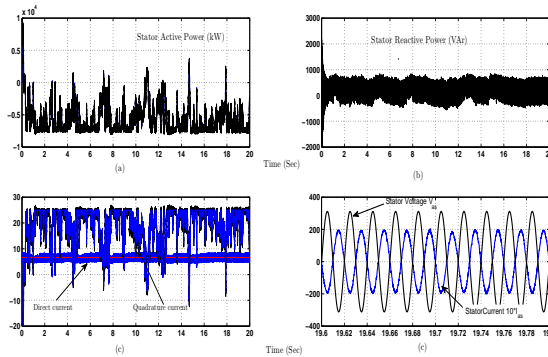


Figure 8: (a), (b) show the stator active and reactive power, (c) rotor direct and quadrature currents, (d) zoom in the stator current and grid voltage.

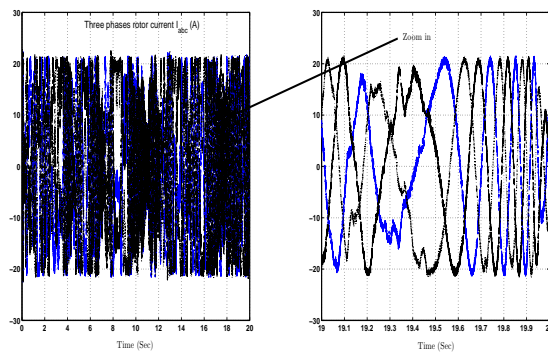


Figure 9: (a) shows rotor currents, (b) zoom in rotor currents.

5 Conclusion

In this paper, we set the higher-order sliding mode control of an energy conversion system based on the double-fed asynchronous machine. In the first step, a model of the wind turbine was proposed. Next, a control strategy by sliding mode of the wind turbine assuming an independent control of power has been recommended. Regulators of active and reactive power by sliding mode have been proposed and tested. The simulation results allowed us to determine the properties of the sliding mode control. Through the simulation results and, specifically, the response of the active and reactive power, there are good performances even in the presence of variation orders. Note that there is a sudden change during the transient. The continuation in power is perfect. The stability and convergence to the equilibrium is assured. In addition, for these types of adjustment (sliding mode) a practical control algorithm is robust and simple to implement.

Acknowledgment

The research is part of a project CNEPRU (refs :A01L07U260 1200150005, Jan 2016), realized in the laboratory of electrical engineering and automatic LREA research, University of Medea, Algeria.

References

- [1] A. Moualdia, M.O. Mahmoudi and L. Nezli. Direct torque control of the DFIG and direct power control for grid side converter in wind power generation system. *The Mediterranean Journal of Measurement and Control, MEDJMC* **9**(3) (2013) 101–108.
- [2] ER. Sanseverino, Di. Sanseverino, ML. Silvestre, MG. Ippolito and De. Paola. An execution, monitoring and replanting approach for optimal energy management in micro-grids. *Energy* **36**(5) (2011) 3429–3436.
- [3] A. Rabiee, H. Khorramdel and A. Aghaei. A review of energy storage systems in micro-grids with wind turbines. *Renewable and Sustainable Energy Reviews* **18** (2) (2013) 316–326.
- [4] A. Chalanga, S. Kamal and B. Moreno. Implementation of super-twisting control: super-twisting and higher order sliding-mode observer-based approaches. *IEEE Trans. Industrial Electronics* **63**(6) (2016) 3677–3685.
- [5] G. Bartolini, A. Ferrara and E. Usai. Chattering avoidance by second-order sliding mode control. *IEEE Trans. on Automatic Control* **43** (2)(1998) 241–246.
- [6] H. Pan and X. Chen. Global robust optimal sliding mode control for uncertain affine nonlinear systems. *Journal of Systems Engineering and Electronics* **20**(4)(2009) 838–843.
- [7] V. Utkin. Discussion aspects of high-order sliding mode control. *IEEE Trans. Automatic Control* **61** (3)(2016) 829–833.
- [8] C. Wang and H. Yau. Nonlinear dynamic analysis and sliding mode control for a gyroscope system. *Nonlinear Dynamics*. **66**(1–2)(2013) 53–65.

- [9] Y. Shtessel and L. Shkolnikov. An Asymptotic Second-Order Smooth Sliding Mode Control. *Asian Journal of Control.* **5**(4) (2003) 498–504.
- [10] ZH. Ismail and VW. Putranti. Second order sliding mode control scheme for an autonomous underwater vehicle with dynamic region concept. *Mathematical Problems in Engineering* **42**(12) (2015) 1–13.
- [11] A. Tlemcani, K. Sebaa and N. Henin. Indirect adaptive fuzzy control of multivariable non-linear systems class with unknown parametres. *Nonlinear Dynamics and Systems Theory* **14**(2) (2014) 162–174.
- [12] T. Chiew, Z. Jamaludin, AB. Hashim, K. LLeo, A. Abdullah and N. Rafan. Analysis of tracking performance in machine tools for disturbance forces compensation using sliding mode control and PID controller. *International Journal of Mechanical and Mechatronics Engineering*. **12** (2012) 34–40.
- [13] M. Liserre, R. Cardenas, M. Molinas and J. Rodriguez. Overview of multi-MW wind turbines and wind parks. *IEEE Trans. Ind. Electron.* **58**(4) (2011) 1081–1095.
- [14] F. Valenciaga and P.F. Puleston. Variable structure control of a wind energy conversion system based on a brushless doubly fed reluctance generator. *IEEE Trans. Energy Convers* **22**(2) (2008) 499–506.
- [15] M. Tazil, V. Kumar, R.C. Bansal, S. Kong, Z.Y. Dong, W. Freitas, and H.D. Mathur. Three-phase doubly fed induction generators: An overview. *IET Elect. Power Appl.* **04**(2) (2010) 75–89.
- [16] F. Hamidia, A. Abadi, A. Tlemcani and M.S. Boucherit. Dual star induction motor supplied with double photovoltaic panels based on fuzzy logic type-2. *Nonlinear Dynamics and Systems Theory* **18**(4) (2018) 359–371.
- [17] A. Abadi, H. Hamidia, A. Morsli and A. Tlemcani. Optimal voltage controller using T-S fuzzy model for multimachine powersystems. *Nonlinear Dynamics and Systems Theory* **19**(2) (2019) 217–226.
- [18] H. Hamidia, A. Larabi, A. Tlemcani and M.S. Boucherit. AIDTC Techniques for Induction Motors. *Nonlinear Dynamics and Systems Theory* **13**(2) (2013) 147–156.
- [19] S. Bentouati, A. Tlemcani, M.S. Boucherit and L. Barasane. A DTC Neurofuzzy Speed Regulation Concept for a Permanent Magnet Synchronous Machine. *Nonlinear Dynamics and Systems Theory* **13**(4) (2013) 344–358.